Frequency-domain synchronization of structural health monitoring data

Kosmas Dragos[1], Filipe Magalhães[2], George D. Manolis[3] and Kay Smarsly[1]

[1]Institute of Digital and Autonomous Construction, Hamburg University of Technology, Blohmstraße 15, 21079 Hamburg, Germany

[2]CONSTRUCT – ViBest, Faculty of Engineering, University of Porto, Rua Dr. Roberto Frias, 4200-465 Porto, Portugal

[3]Laboratory of Experimental Mechanics, Department of Civil Engineering, Aristotle University, 54124 Thessaloniki, Greece

Abstract

Since the advent of structural health monitoring (SHM), vibration analysis has been one of the most popular strategies for yielding modal information of structures, such as eigenfrequencies and mode shapes. As a result of the relatively high sampling rates adopted in vibration analysis, obtaining accurate modal information requires absolute synchronization of structural response data. Despite the advances in sensing technologies and synchronization protocols, synchronization discrepancies in structural response data may occur due to drifting in internal clocks of independent data acquisition units. Particularly in wireless SHM, in which each wireless sensor node essentially operates as an independent data acquisition unit, mitigating clock drifting has been an area of intensive research. This paper addresses the issue of data synchronization from a physics-based perspective, aiming to add an additional synchronization check at the post-sampling stage. Specifically, a frequency-domain synchronization approach is reported, which builds upon the relationship between time lags in structural response data and the cross spectral density phase angles. Validation tests are conducted using simulations of a multi-degree-of-freedom oscillator and data collected from a full-scale road bridge, demonstrating the capability of the approach to estimate time lags between SHM data even in the presence of non-proportional damping, thus overcoming a common limitation of other synchronization methods. The frequency-domain synchronization approach is intended to complement synchronization protocols in extracting accurate modal information.

Keywords: Synchronization, structural health monitoring, cross spectral density, frequency-domain analysis.

1. Introduction

The crucial cornerstone of most structural health monitoring (SHM) strategies is the reliability of information extracted from structural response data [1]. The information is usually the outcome of

system identification methods, which provide practitioners with insights into the structural properties of civil infrastructure. Particularly in vibration-based SHM, structural dynamic properties, such as eigenfrequencies and mode shapes, may severely be affected by inaccuracies in the structural response data, which, in turn, could lead to misjudgments of structural condition [2]. Therefore, maintaining high levels of reliability in structural response data is of paramount importance in SHM [3].

While inaccuracies in structural response data could stem from various sources, a frequent challenge in modern vibration-based SHM is to ensure absolute synchronization in the data ("data synchronization"). Considering the tethered, centralized setup of traditional SHM systems, data synchronization seems, at a first glance, for granted; nonetheless, synchronization discrepancies have been increasingly affecting modern SHM systems. On the one hand, rapidly evolving trends in SHM have been fostering the transition from cable-based SHM to wireless SHM, which is implemented via wireless sensor nodes that lack inherent global clock management [4]. On the other hand, malfunctions, e.g., of analog-to-digital converters or the use of multiple parallel data acquisition units could cause synchronization discrepancies even in cable-based SHM systems [5]. Especially wireless sensor networks and wireless SHM systems are being increasingly considered integral parts of Internet-of-Things applications, developed within emerging technological paradigms such as smart cities and Industry 4.0, in which the importance of data synchronization is emphasized [6-7]. In vibration-based SHM, which usually involves high sampling frequencies, synchronization discrepancies may compromise the accuracy of experimentally identified mode shapes and result in erroneous system identification [8].

An apparent solution to synchronization discrepancies is to implement protocols for ensuring global clock management among wireless sensor nodes or data acquisition units [9-10]. Global clock management is usually assigned to middleware-driven network-wide communication protocols, thus averting synchronization discrepancies already at the commencement stage of network operation. A large body of research can be found in literature, proposing synchronization protocols mainly for wireless sensor networks. Seminal works include the reference-based synchronization protocol introduced by Elson et al. [11], the timing-sync protocol for sensor networks proposed by Ganeriwal et al. [12], and the flooding time synchronization protocol presented by Maróti et al. [13]. From a broad wireless sensor network synchronization perspective, most research works focus on improving the aforementioned protocols by reducing the wireless communication overhead required to synchronize wireless sensor nodes. Examples include the adaptive time synchronization protocol reported by Chauhan and Awasthi [14], the gradient time synchronization protocol introduced by Sommer and Wattenhofer [15], and the adaptive value tracking protocol suggested by Yildirim and Gürcan [16].

The concept of assigning synchronization tasks to network-wide communication via middleware services of wireless sensor nodes has been extended to wireless SHM [17]. For example, the prototype implementations presented by Rice and Spencer [18] and Nagayama et al. [19] utilize synchronization middleware services of the Imote2 wireless sensor node, and the prototype sensor node presented by Wang et al. [20] implements point-to-multipoint communication for synchronization. Other synchronization approaches related to wireless SHM include the μ-sync protocol introduced by Bocca et al. [21], which has been proven to keep the synchronization error

under 10 μs, and the autoregressive models proposed by Lei et al. [22] for estimating time delays between input loads and output structural response data or between output structural response data from different locations. In synchronizing wireless sensor nodes for SHM, a major challenge emphasized by several researchers is to keep algorithms and protocols relatively "lightweight" so as to preserve the limited resources of the sensor nodes. In this direction, Sazonov et al. [23] have suggested a two-tier synchronization scheme, in which low-level sensor nodes are organized in clusters synchronized by so-called "coordinator" nodes, while coordinator nodes themselves synchronize their internal clocks using global positioning system technologies. Moreover, Chintalapudi et al. [24], have proposed synchronizing structural response data by timestamping the data after being collected at a "gateway" sensor node, instead of conducting network-wide synchronization. The aforementioned approaches have been implemented in practical applications, involving wireless SHM of masonry structures [25], heritage structures [26], and bridges [27]. Furthermore, notable practical approaches on synchronization may also be found in SHM application areas beyond structural engineering, such as vehicular monitoring [28], aircraft monitoring [29], and railway monitoring [30].

Despite the effectiveness of clock synchronization approaches, the consensus of SHM researchers suggest that clock synchronization can hardly guarantee synchronized sensing in vibration-based SHM [31-32]. Acceleration response data from structural vibrations is usually collected at relatively high sampling frequencies and for long sampling periods, e.g. as compared to environmental data. As a result, vibration-based SHM is prone to random delays caused by microcontrollers of wireless sensor nodes or data acquisition units, to fluctuations in the sampling frequency, and to clock drifting over time. Therefore, synchronization discrepancies may still infiltrate the structural response data and can only be addressed through post-processing. For example, estimating synchronization discrepancies based on correlations in structural response data has been proposed by Brincker and Brandt [33]. Furthermore, using phase differences at modal frequency components of structural response data to estimate synchronization discrepancies has been the focus of works conducted by Maes et al. [34], Dragos et al. [35-36], and Bernal [37]. However, the previously mentioned "phase-based" approaches are limited to individual modal frequency components.

This paper aims at generalizing the phase-based estimation of synchronization discrepancies by leveraging a large part of the "bandwidth of interest", i.e. the number of frequency components practically constituting the frequency content of the structural response. In essence, the frequency-domain synchronization ("FD-Sync") approach discussed herein extends the concept presented in [35] by integrating and mathematically formalizing the relationship between a synchronization discrepancy ("time lag") and the slope of the cross spectral density phase spectrum of two SHM data records, containing acceleration response data, which has been described by Diord et al. [38]. The purpose of the FD-Sync approach is to increase the accuracy of estimates of vibration-based SHM information, such as mode shapes, relying exclusively on frequency-domain analysis of structural response data. It should be noted that in practical applications, frequency-domain analysis is inherently approximative, and its results, e.g. spectral density functions, are usually affected by ambient noise and quantization errors. By extension, the FD-Sync approach is also approximative and is intended to complement existing synchronization approaches, rather than estimate time delays to the order of microseconds. As a result, the approximative character of the

FD-Sync approach is also investigated in this paper, along with the applicability limits in terms of time lag detection, through simulations on a simple numerical model. Finally, validation tests are conducted on structural response data collected from a long-term SHM system installed on a road bridge.

The remainder of the paper is organized as follows: In Section 2, the mathematical formulation of the relationship between synchronization discrepancies and cross spectral density phase spectra is illuminated. Section 3 covers the simulations performed to investigate the applicability limits of the FD-Sync approach, and Section 4 presents the validation tests. Finally, the main points of this study are summarized, the conclusions are highlighted, and a brief outlook on future research is provided.

2. Relationship between synchronization discrepancies and cross spectral density phase

The FD-Sync approach builds upon the relationship between phase angles of structural response data records collected from different locations of a structure being monitored. In this section, the mathematical background of the proposed approach is illuminated using a simple example of two SHM data records.

SHM data records containing acceleration response data are collected in the form of digitized signals that can be treated as superpositions of several harmonic sinusoidal functions. The number of harmonic sinusoidal functions contained in each signal is theoretically governed by the frequency bandwidth of data collection, which, in turn, is associated with the sampling frequency. Nevertheless, in civil engineering structures, only a few harmonic sinusoidal functions, corresponding to vibration modes ("vibration mode components"), exhibit non-negligible contributions to structural responses, while the rest are considered noise components. Considering the disaggregation of SHM data records into vibration mode components, time lags between two records are reflected in phase angle relationships between individual vibration mode components. Specifically, in conventional lightly-damped civil engineering structures, phase angle differences between vibration mode components are either close to zero or close to π, depending on the vibration mode topology, which determines whether vibration mode components from different records are positively or negatively correlated [39]. Figure 1 shows how a time lag τ between two signals g_1 and g_2 affects the phase angle differences $\Delta\theta_i$ of individual vibration mode components h_{1i} and h_{2i} ($i = 1,2,\ldots,m$). In the example of Figure 1, the expected phase differences for vibration mode components 1, 2, and m are $\Delta\theta_1 = 0$, $\Delta\theta_2 = \pi$, $\Delta\theta_m = 0$.

Considering signals g_1 and g_2 as superpositions of m vibration mode components, the following expressions are obtained:

$$\begin{aligned} g_1(t) &= \sum_{q=1}^{m} R_{1q} \sin\left(2\pi f_q t + \theta_{1q}\right) \\ g_2(t) &= \sum_{q=1}^{m} R_{2q} \sin\left(2\pi f_q t + \theta_{2q}\right) \end{aligned} . \tag{1}$$

In Equation 1, f_q is the frequency, R_q is the amplitude and θ_q is the arbitrary phase angle, respectively, of the qth vibration mode component contributing to the structural response, and t is the time. Signals are usually discretized into N-sized time series at constant time intervals Δt and analyzed in the frequency domain, using the fast Fourier transform (FFT). Furthermore, the relationship between two signals in the frequency domain is usually investigated by means of the cross spectral density function between the signals. It is therefore expected that phase differences occurring as a result of synchronization discrepancies between two signals are reflected in the phase angles of the spectral density function.

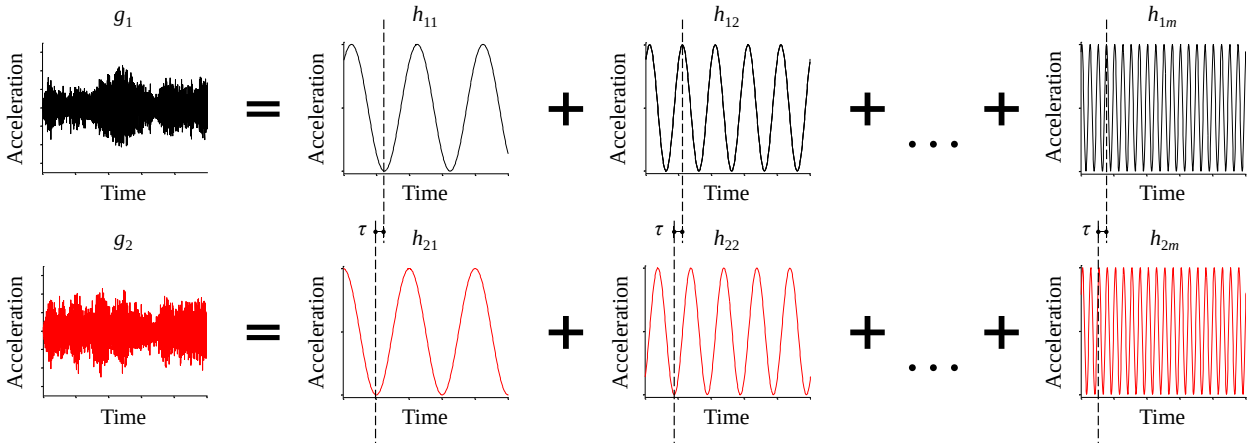

Figure 1: Time lag between signals g_1 and g_2.

In what follows, the connection between synchronization discrepancies and spectral density phase angles will be mathematically described. First, the N-sized signals g_1 and g_2 are transformed into the frequency domain using the FFT, the kth harmonic sinusoidal function G_k of which is obtained from:

$$\begin{aligned}\mathcal{F}_k(g_1) &= G_{k1} = \sum_{q=1}^{m}\sum_{n=0}^{N-1} R_{1q}\sin\left(2\pi f_q n\Delta t + \theta_{1q}\right)\cdot e^{-i2\pi k\,n/N} \\ \mathcal{F}_k(g_2) &= G_{k2} = \sum_{q=1}^{m}\sum_{n=0}^{N-1} R_{2q}\sin\left(2\pi f_q n\Delta t + \theta_{2q}\right)\cdot e^{-i2\pi k\,n/N}.\end{aligned} \tag{2}$$

Using Euler's identity, the expressions in Equation 2 are modified as follows:

$$\begin{aligned}\mathcal{F}_k(g_1) &= G_{k1} = 1/2i\sum_{q=1}^{m} R_{1q}\sum_{n=0}^{N-1}\left(e^{i\left(2\pi f_q n\Delta t+\theta_{1q}\right)} - e^{-i\left(2\pi f_q n\Delta t+\theta_{1q}\right)}\right)\cdot e^{-i2\pi k\,n/N} \\ \mathcal{F}_k(g_2) &= G_{k2} = 1/2i\sum_{q=1}^{m} R_{2q}\sum_{n=0}^{N-1}\left(e^{i\left(2\pi f_q n\Delta t+\theta_{2q}\right)} - e^{-i\left(2\pi f_q n\Delta t+\theta_{2q}\right)}\right)\cdot e^{-i2\pi k\,n/N},\end{aligned} \tag{3}$$

which is further transformed to:

$$\mathcal{F}_k(g_1) = G_{k1} = 1/2i \sum_{q=1}^{m} R_{1q} \left[e^{i\theta_{1q}} \sum_{n=0}^{N-1} e^{i2\pi n\left(f_q \Delta t - k/N\right)} - e^{-i\theta_{1q}} \sum_{n=0}^{N-1} e^{-i2\pi n\left(f_q \Delta t + k/N\right)} \right]$$
$$\mathcal{F}_k(g_2) = G_{k2} = 1/2i \sum_{q=1}^{m} R_{2q} \left[e^{i\theta_{2q}} \sum_{n=0}^{N-1} e^{i2\pi n\left(f_q \Delta t - k/N\right)} - e^{-i\theta_{2q}} \sum_{n=0}^{N-1} e^{-i2\pi n\left(f_q \Delta t + k/N\right)} \right]. \quad (4)$$

To simplify the exponential summations, the geometric sum formula is used:

$$\Sigma_1 = \sum_{n=0}^{N-1} e^{i\xi n} = 1 + e^{i\xi} + \ldots + e^{i(N-1)\xi} \Leftrightarrow \Sigma_2 = \frac{\Sigma_1}{e^{i\xi}} = e^{-i\xi} + 1 + e^{i\xi} + \ldots + e^{i(N-2)\xi}$$
$$\Sigma_1 - \Sigma_2 = \Sigma_1 - \frac{\Sigma_1}{e^{i\xi}} = -e^{-i\xi} + e^{i(N-1)\xi} \Leftrightarrow \Sigma_1 = \frac{-e^{-i\xi} + e^{i(N-1)\xi}}{1 - e^{-i\xi}} = \frac{-1 + e^{iN\xi}}{e^{i\xi} - 1} = \frac{1 - e^{iN\xi}}{1 - e^{i\xi}}, \quad (5)$$

which, using Euler's identity again, is further simplified as:

$$\Sigma_1 = \sum_{n=0}^{N-1} e^{i\xi n} = \frac{1 - e^{iN\xi}}{1 - e^{i\xi}} = \frac{e^{i N/2 \xi}\left(e^{-i N/2 \xi} - e^{i N/2 \xi}\right)}{e^{i 1/2 \xi}\left(e^{-i 1/2 \xi} - e^{i 1/2 \xi}\right)} = \frac{\sin\left(N/2 \xi\right)}{\sin\left(1/2 \xi\right)} e^{i (N-1)/2 \xi}. \quad (6)$$

Plugging Equation 6 into Equation 4, the FFT expressions are modified into:

$$G_{k1} = \frac{1}{2i} \sum_{q=1}^{m} R_{1q} \left[e^{i\theta_{1q}} \frac{\sin\left(\pi\left(f_q N \Delta t - k\right)\right)}{\sin\left(\pi\left(f_q \Delta t - k/N\right)\right)} e^{i2\pi\left(f_q \Delta t - k/N\right)\frac{(N-1)}{2}} - e^{-i\theta_{1q}} \frac{\sin\left(-\pi\left(f_q N \Delta t + k\right)\right)}{\sin\left(-\pi\left(f_q \Delta t + k/N\right)\right)} e^{-i2\pi\left(f_q \Delta t + k/N\right)\frac{(N-1)}{2}} \right]$$
$$G_{k2} = \frac{1}{2i} \sum_{q=1}^{m} R_{2q} \left[e^{i\theta_{2q}} \frac{\sin\left(\pi\left(f_q N \Delta t - k\right)\right)}{\sin\left(\pi\left(f_q \Delta t - k/N\right)\right)} e^{i2\pi\left(f_q \Delta t - k/N\right)\frac{(N-1)}{2}} - e^{-i\theta_{2q}} \frac{\sin\left(-\pi\left(f_q N \Delta t + k\right)\right)}{\sin\left(-\pi\left(f_q \Delta t + k/N\right)\right)} e^{-i2\pi\left(f_q \Delta t + k/N\right)\frac{(N-1)}{2}} \right]. \quad (7)$$

To simplify notation, the following equalities are defined:

$$A_{qk} = \frac{\sin\left(\pi\left(f_q N \Delta t - k\right)\right)}{\sin\left(\pi\left(f_q \Delta t - k/N\right)\right)} \qquad B_{qk} = \frac{\sin\left(-\pi\left(f_q N \Delta t + k\right)\right)}{\sin\left(-\pi\left(f_q \Delta t + k/N\right)\right)},$$
$$a_{qk} = 2\pi\left(f_q \Delta t - k/N\right)(N-1)/2 \qquad b_{qk} = 2\pi\left(f_q \Delta t + k/N\right)(N-1)/2. \quad (8)$$

With the equalities specified above, the FFT expressions of the two signals are:

$$G_{k1} = 1/2i \sum_{q=1}^{m} R_{1q} \left[e^{i\theta_{1q}} A_{qk} e^{i a_{qk}} - e^{-i\theta_{1q}} B_{qk} e^{-i b_{qk}} \right]$$
$$G_{k2} = 1/2i \sum_{q=1}^{m} R_{2q} \left[e^{i\theta_{2q}} A_{qk} e^{i a_{qk}} - e^{-i\theta_{2q}} B_{qk} e^{-i b_{qk}} \right]. \quad (9)$$

The cross spectral density function between signals g_1 and g_2 is given in Equation 10.

$$S_{k12} = G_{k1} \cdot G_{k2}^*, \quad (10)$$

where (*) denotes complex conjugate. Further analysis of Equation 10 results in:

$$S_{k12} = 1/4 \sum_{q=1}^{M} \sum_{j=1}^{M} R_{1i} R_{2j} \cdot \left[\mathrm{Re}(S_{12k}) + i\,\mathrm{Im}(S_{12k}) \right]$$

$$\begin{aligned} \mathrm{Re}(S_{12k}) = {} & A_{qk} A_{jk} \cos\left(\theta_{1q} - \theta_{2j} + a_{qk} - a_{jk}\right) + B_{qk} B_{jk} \cos\left(\theta_{1q} - \theta_{2j} + b_{qk} - b_{jk}\right) - \\ & A_{qk} B_{jk} \cos\left(\theta_{1q} + \theta_{2j} + a_{qk} + b_{jk}\right) - A_{jk} B_{qk} \cos\left(\theta_{1q} + \theta_{2j} + a_{jk} + b_{qk}\right) + \\ \mathrm{Im}(S_{12k}) = {} & A_{qk} A_{jk} \sin\left(\theta_{1q} - \theta_{2j} + a_{qk} - a_{jk}\right) - B_{qk} B_{jk} \sin\left(\theta_{1q} - \theta_{2j} + b_{qk} - b_{jk}\right) - \\ & A_{qk} B_{jk} \sin\left(\theta_{1q} + \theta_{2j} + a_{qk} + b_{jk}\right) + A_{jk} B_{qk} \sin\left(\theta_{1q} + \theta_{2j} + a_{jk} + b_{qk}\right). \end{aligned} \tag{11}$$

From Equation 11, it is evident that the exact computation of the cross spectral density function requires knowledge of the exact frequencies of all vibration mode components ("eigenfrequencies") contributing to the structural response so as to obtain values of A_k, B_k, a_k, and b_k. However, in practical applications, the eigenfrequencies of structures are generally unknown. Rather, SHM practitioners estimate the natural frequencies of structures directly from the FFT expressions of structural response data. Moreover, since the FD-Sync approach presented herein is intended for practical SHM applications, it is reasonable to consider frequencies matching the frequency "bins" (each bin denoted by index k, with frequency $f_k = k/(N\Delta t)$) of the FFT. As a result, assuming a vibration component frequency $f_o = k_o/(N\Delta t)$, the expressions for A_k, B_k, a_k and b_k, are:

$$\begin{aligned} A_{k_o} &= \lim_{k \to k_o} \frac{\sin\left(\pi\left(f_o N\Delta t - k\right)\right)}{\sin\left(\pi\left(f_o \Delta t - k/N\right)\right)} \qquad\qquad \xi = \pi\left(f_o \Delta t - k/N\right), \\ A_{k_o} &= \lim_{\xi \to 0} \sum_{\kappa=0}^{N} \binom{N}{\kappa} \left(\cos^{\kappa} \xi\right) \left(\sin^{N-\kappa-1} \xi\right) \sin\left[\tfrac{1}{2}\left(N - \kappa\right)\right] \pi = N, \end{aligned} \tag{12}$$

$$B_{k_o} = \frac{\sin\left(-\pi\left(f_o N\Delta t + k_o\right)\right)}{\sin\left(-\pi\left(f_o \Delta t + k_o/N\right)\right)} = \frac{\sin\left[-2\pi k_o\right]}{\sin\left(-2\pi k_o/N\right)} = 0, \tag{13}$$

$$a_{k_o} = 2\pi\left(f_o \Delta t - k_o/N\right)\left(N-1\right)/2 = 0, \tag{14}$$

$$b_{k_o} = 2\pi\left(f_o \Delta t + k_o/N\right)\left(N-1\right)/2 = \pi k_o\left(1 - 1/N\right). \tag{15}$$

It should be noted that obtaining the value for A_k from Equation 15 is possible only for the frequency components closest to frequency bin k, i.e. for $k_x \neq k$, the nominator in Equation 12 becomes a sine of an integer multiple of 2π, resulting in $A_{qkx} = A_{jkx} = 0$. Therefore, Equation 11 is computed only for $k = q = j$, which, using Equations 12-15, is reduced to:

$$S_{12k} = 1/4 \cdot N^2 \cdot R_{1k} R_{2k} \cdot \left[\cos\left(\theta_{1k} - \theta_{2k}\right) + i \sin\left(\theta_{1k} - \theta_{2k}\right)\right] \tag{16}$$

The phase angle of the spectral density function is computed as follows:

$$\angle S_{12k} = \varphi_k = \tan^{-1}\left[\frac{\sin\left(\theta_{1k} - \theta_{2k}\right)}{\cos\left(\theta_{1k} - \theta_{2k}\right)}\right], \tag{17}$$

The time lag τ can be expressed as a phase angle θ added to the arbitrary phase angle $\hat{\theta}_2$ of signal g_2:

$$\begin{aligned} g_2 &= \sum_{j=1}^{m} R_{2j} \sin\left(2\pi f_j n\Delta t + \theta_{2j}\right) = \sum_{j=1}^{m} R_{2j} \sin\left(2\pi f_j n\Delta t + \hat{\theta}_{2j} + \theta\right) \\ \theta_{2j} &= \hat{\theta}_{2j} + 2\pi f_j \tau \Leftrightarrow \tau = \frac{\theta}{2\pi f_j} \end{aligned} . \tag{18}$$

Plugging Equation 18 into Equation 17 eventually results in:

$$\tan\varphi_k = \left[\frac{\sin\left(\theta_{1k} - \hat{\theta}_{2k}\right) - \cos\left(\theta_{1k} - \hat{\theta}_{2k}\right)\tan\theta}{\cos\left(\theta_{1k} - \hat{\theta}_{2k}\right) + \sin\left(\theta_{1k} - \hat{\theta}_{2k}\right)\tan\theta}\right] \qquad \theta \neq \eta\pi,\ \eta = 1,3,5... \tag{19}$$

$$\tan\varphi_k = -\tan\theta \frac{\cos\left(\theta_{1k} - \hat{\theta}_{2k}\right)}{\cos\left(\theta_{1k} - \hat{\theta}_{2k}\right) + \sin\left(\theta_{1k} - \hat{\theta}_{2k}\right)\tan\theta} + \frac{\sin\left(\theta_{1k} - \hat{\theta}_{2k}\right)}{\cos\left(\theta_{1k} - \hat{\theta}_{2k}\right) + \sin\left(\theta_{1k} - \hat{\theta}_{2k}\right)\tan\theta} \tag{20}$$

In theory, civil engineering structures are usually analyzed under the assumption that damping is proportional to mass and stiffness, which would entail arbitrary phase differences being equal to either zero or π depending on the correlation between vibration mode components, as shown in Figure 1. In practice, damping in structural responses is far too complicated to be described explicitly as proportional [40]. Nonetheless, the deviation of actual damping from proportional damping is usually low for operational conditions investigated in SHM, therefore, the arbitrary phase differences for frequency bin *k*, may be approximated as:

$$\cos\left(\theta_{1k} - \hat{\theta}_{2k}\right) \approx \pm 1 \qquad \sin\left(\theta_{1k} - \hat{\theta}_{2k}\right) \approx 0 \tag{21}$$

Using Equations 21 and 24, the expression linking the phase angle of the spectral density function (φ_k) to the time lag τ between signals g_1 and g_2 is obtained:

$$\begin{aligned} &\tan\varphi_k \approx -\tan\theta \Leftrightarrow \theta \approx -\varphi_k + \beta\pi \\ &\Leftrightarrow \tau \approx -\frac{\varphi_k + \beta\pi}{2\pi f_k} \qquad \beta \in \mathbb{Z} \end{aligned} . \tag{22}$$

In the following section, the time lag estimation expression of Equation 22 is used as a basis for developing the FD-Sync approach presented in this paper.

3. Frequency-domain synchronization based on cross spectral density phase spectra

In this section, the practical aspects of the FD-Sync approach are explained through simulations of a simple 5-degree-of-freedom (DOF) oscillator, shown in Figure 2. First, the oscillator properties are described, followed by the techniques used to counteract inaccuracies stemming from the approximative character of Equation 22 and of the FFT. Next, the applicability limits of the FD-Sync approach, in terms of time lag estimation, are investigated by simulating time lags in the structural response data of the oscillator.

3.1. Simulation of a 5-DOF oscillator

The oscillator used for the simulations comprises 5 masses lumped at discrete points that are connected with beam elements. Modeling follows the "stick model" paradigm, i.e. only one-direction translational degrees of freedom (x_i, $i = 1…5$) are considered for each mass, as shown in Figure 2a. The oscillator is subjected to forced vibration with a triangular load profile and Gaussian white noise functions as "load histories". To avoid correlation among the load histories, a different random Gaussian function is generated for each load history and each simulation. The simulations are performed by solving the equation of motion:

$$\mathbf{M}\ddot{\mathbf{x}} + \mathbf{C}\dot{\mathbf{x}} + \mathbf{K}\mathbf{x} = \mathbf{P}\,, \tag{23}$$

where **M** is the mass matrix of the oscillator, **C** is the damping matrix, **K** is the stiffness matrix, and $\ddot{\mathbf{x}}$, $\dot{\mathbf{x}}$, **x**, **P** are the acceleration vector, the velocity vector, the displacement vector and the load vector, respectively. Since the proportional damping assumption in real-world structures is an approximation that could compromise the accuracy of Equations 21 and 22, two sets of trial simulations are conducted, TS_1 and TS_2, considering both proportional damping and non-proportional damping. Specifically, the proportional damping matrix $\mathbf{C}_{pr}$ is first estimated using the Rayleigh coefficients a_1, a_2 for a constant damping ratio of ζ = 2‰ at the first two eigenfrequencies (f_1, f_2) of the oscillator:

$$\mathbf{C}_{pr} = a_1\mathbf{M} + a_2\mathbf{K}, \qquad a_1 = 4\pi\zeta\frac{f_1 f_2}{f_1 + f_2} \qquad a_2 = \frac{\zeta}{\pi\left(f_1 + f_2\right)}. \tag{24}$$

Subsequently, a tuned mass damper (TMD) is added to the top mass of the oscillator to counteract the fundamental vibration mode (Figure 2b). Drawing from TMD theory, the TMD reduces oscillation amplitudes by responding in an out-of-phase manner with respect to the structure, thus introducing a phase shift between the response of the top mass (DOF x_5) and of the TMD. For the sake of simplicity, the TMD parameters m_d, c_d, and k_d are computed according to Den Hartog [41], resulting in a constant phase shift between the TMD and the structure at the tuning frequency. The addition of the TMD damping parameter c_d to the damping matrix $\mathbf{C}_{pr}$ results in non-proportional damping matrix $\mathbf{C}_{np}$.

The value of the load profile at DOF r ($r = 1\ldots5$) is defined as: $P_r(t) = z_r \cdot P \cdot w_r(t)$, where $P = 100$ kN, z_r is a load factor, and w_r is the load history with $w_r \sim N(0,1)$. The mass and stiffness parameters of the oscillator, as well as the load factors and the five eigenfrequencies are summarized in Table 1.

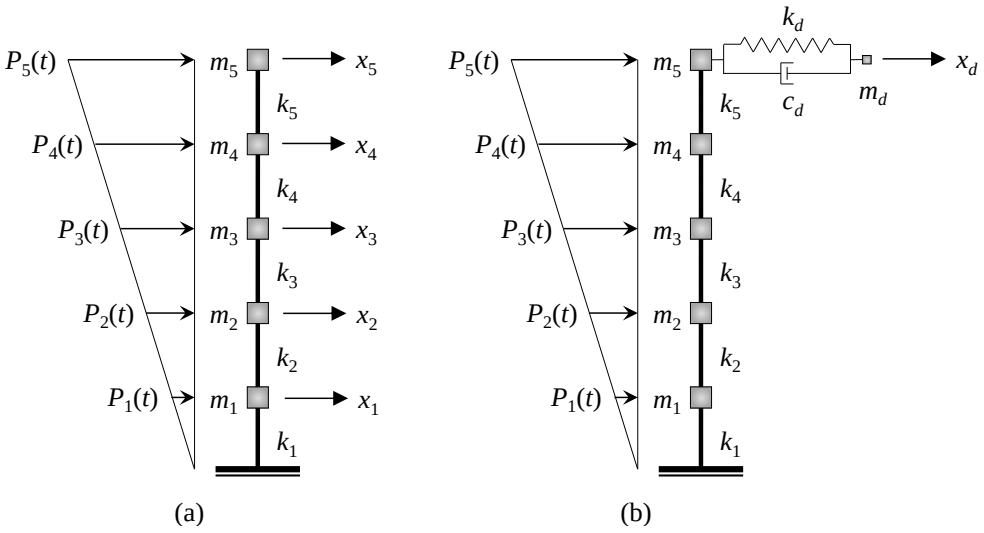

Figure 2: Stick model 5-DOF oscillator used for simulations.

Table 1: Mass, stiffness parameters, load factors and eigenfrequencies of the oscillator.

Structural properties				**Eigenfrequencies**	
r	m_r (t)	k_r (kN/m)	z_r (-)	Mode	f (Hz)
1	40	$150 \cdot 10^3$	0.2	1	3.21
2	30	$100 \cdot 10^3$	0.4	2	8.25
3	25	$100 \cdot 10^3$	0.6	3	12.38
4	20	$100 \cdot 10^3$	0.8	4	15.75
5	20	$75 \cdot 10^3$	1.0	5	19.15

The TMD parameters are computed for suppressing the fundamental eigenfrequency $f_1 = 3.21$ Hz, which has a modal mass of $\tilde{m}_1 = 59.15$ t. Considering a TMD mass percentage ratio of 4% of the modal mass of the fundamental frequency:

$$\mu = \frac{m_d}{\tilde{m}_1} = 0.04 \quad \zeta_d = \sqrt{\frac{3\mu}{8(1+\mu)}} \approx 12\% \quad f_{opt} = \frac{\omega_d}{\omega_1} = \frac{1}{1+\mu} \approx 0.9615$$
$$m_d = \mu \cdot \tilde{m}_1 = 2.366 \text{ t} \qquad \omega_d = 3.21 \cdot 2\pi \cdot 0.9615 \quad k_d = \omega_d^2 \cdot m_d \approx 889.78 \text{ kN/m} \tag{25}$$
$$c_d = 2 \cdot \zeta_d \cdot \sqrt{m_d \cdot k_d} \approx 11.00 \text{ kNs/m}.$$

Finally, the expansions of the accelerations, velocities and displacements at time point n are obtained using the Newmark-β algorithm, for $\gamma = 0.5$ and $\beta = 0.25$:

$$\ddot{\mathbf{x}} = \begin{bmatrix} \ddot{x}_1 & \ddot{x}_2 & \dots & \ddot{x}_m \end{bmatrix}, \quad \dot{\mathbf{x}} = \begin{bmatrix} \dot{x}_1 & \dot{x}_2 & \dots & \dot{x}_m \end{bmatrix}, \quad \mathbf{x} = \begin{bmatrix} x_1 & x_2 & \dots & x_m \end{bmatrix}$$
$$\dot{x}_{n+1} = \dot{x}_n + (1-\gamma)\Delta t \cdot \ddot{x}_n + \gamma \Delta t \cdot \ddot{x}_{n+1} \tag{26}$$
$$x_{n+1} = x_n + \Delta t \cdot \dot{x}_n + \tfrac{1}{2}(\Delta t)^2 \left[(1-2\beta) \cdot \ddot{x}_n + 2\beta \cdot \ddot{x}_{n+1} \right].$$

To verify the effect of the TMD on the complexity of mode shapes as a result of non-proportional damping, preliminary simulations are conducted. In particular, two acceleration response data sets are obtained using Equations 23 and 26, one by setting $\mathbf{C} = \mathbf{C}_{pr}$ and one by setting $\mathbf{C} = \mathbf{C}_{np}$. Upon obtaining the acceleration response data sets, two sets of mode shapes, $\boldsymbol{\psi}_{pr} = \{\psi_{pr,j}\}$ and $\boldsymbol{\psi}_{np} = \{\psi_{np,j}\}$ (j = 2…5), respectively, are extracted using the frequency domain decomposition method [42]. The first mode shape is omitted, since the respective eigenfrequency is suppressed by the TMD. The purpose of the preliminary simulations is to show the effect of non-proportional damping on the imaginary parts of mode shapes. Moreover, the reason for extracting mode shapes from acceleration response data instead of using modal analysis methods is to account for approximation errors introduced by the FFT, which may result in non-zero – yet negligible – imaginary parts of mode shapes even in the case of proportional damping. The mode shapes extracted from the preliminary simulations are plotted in the complex plane, as shown in Figure 3, clearly showing that the addition of the TMD to the oscillator results in non-proportional damping, represented by a significant deviation from zero of the imaginary parts of mode shapes $\boldsymbol{\psi}_{np}$.

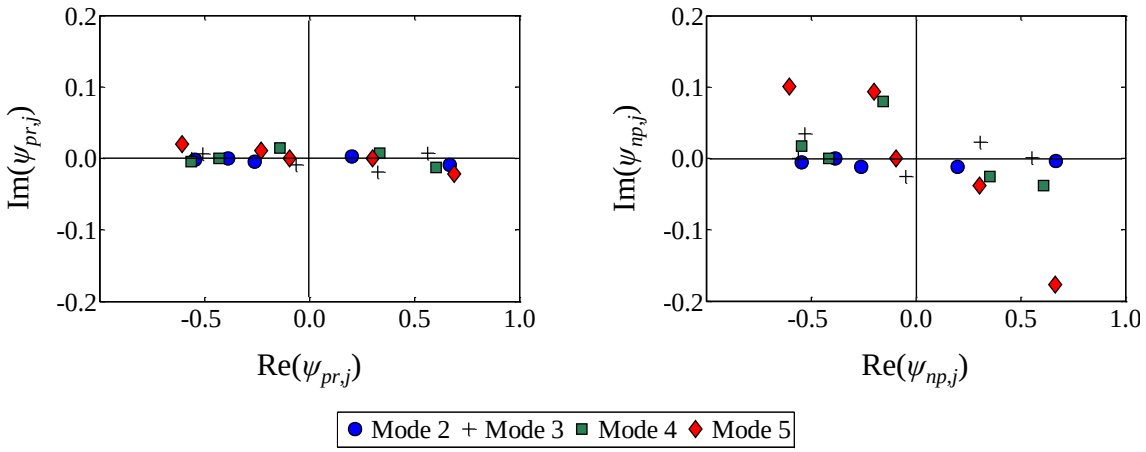

Figure 3: Representation of mode shapes in the complex plane.

3.2. Noise reduction

Signals in SHM are usually contaminated with noise, which is depicted in the frequency-domain representations of the signals through non-smooth FFT and cross spectral density amplitude plots. Sources of noise include external interference, input loads with rich frequency content (quasi-white-noise input), and quantization errors, which are collectively (and approximately) treated as zero-mean random Gaussian processes. To obtain smooth cross spectral density representations,

common SHM practice adopts signal processing techniques, such as windowing and spectral averaging [43]. In general, windowing involves segmenting signals into time series of short lengths, and spectral averaging consists in computing averages of cross spectral density representations of all segments. Witte [43] reports on two spectral averaging methods, (i) "root-mean-square (RMS) averaging", and (ii) "vector averaging". In RMS averaging, the kth component of the average cross spectrum $\tilde{S}_k$ is computed by averaging scalar cross spectral density outputs (amplitudes $|S_k|$ and phase angles $\angle S_k$) of N_s segments, as shown in Equation 27. Vector averaging consists in averaging real parts and imaginary parts of complex cross spectral density values separately for deriving the average cross spectrum, as shown in Equation 28.

$$\left|\tilde{S}_k\right| = \sqrt{\frac{1}{N_s}\sum_{j=1}^{N_s}\left|S_{kj}\right|^2} \qquad \angle\tilde{S}_k = \sqrt{\frac{1}{N_s}\sum_{j=1}^{N_s}\angle S_{kj}^2} \tag{27}$$

$$\mathrm{Re}\left(\tilde{S}_k\right) = \frac{1}{N_s}\sum_{j=1}^{N_s}\mathrm{Re}\left(S_{kj}\right) \qquad \mathrm{Im}\left(\tilde{S}_k\right) = \frac{1}{N_s}\sum_{j=1}^{N_s}\mathrm{Im}\left(S_{kj}\right) \tag{28}$$

RMS averaging reduces the variability of amplitudes and phases, but does not reduce noise levels of signals. By contrast, vector averaging cancels out noise components, but effects poorer smoothing compared to RMS averaging. Figure 4 exemplarily shows the effect of both spectral averaging methods on the cross spectra density phase functions between two signals, representing structural response data from degrees of freedom x_1, x_2 of the oscillator, computed at a sampling frequency of 100 Hz. Phase angles in Figure 4 are plotted against the angular frequency ω_k, since the time lag τ is essentially associated with $2\pi f_k$ in Equation 22. The effect of the time lag τ on the phase angle plot is depicted as a linear "trend", with angle y essentially representing the time lag. Finally, the limitation of phase angles being bounded within $[-\pi, \pi]$ is evidenced by the replication of the linear trend once the upper bound of the phase angle value is reached, which results in the requirement to add an integer multiple of π, as shown in Equation 22. The same replication applies for negative time lags, where the lower bound of the phase angle is reached. Both spectral averaging methods successfully reduce noise levels, while retaining the "meaningful" portions of the signals, i.e. the phase angles within the bandwidth of interest 0-125 rad/s (0-20 Hz) corresponding to the eigenfrequencies of the oscillator. Nonetheless, the vector averaging method exhibits higher noise reduction, which is crucial for accurate time lag detection, and will be used in the remainder of the paper.

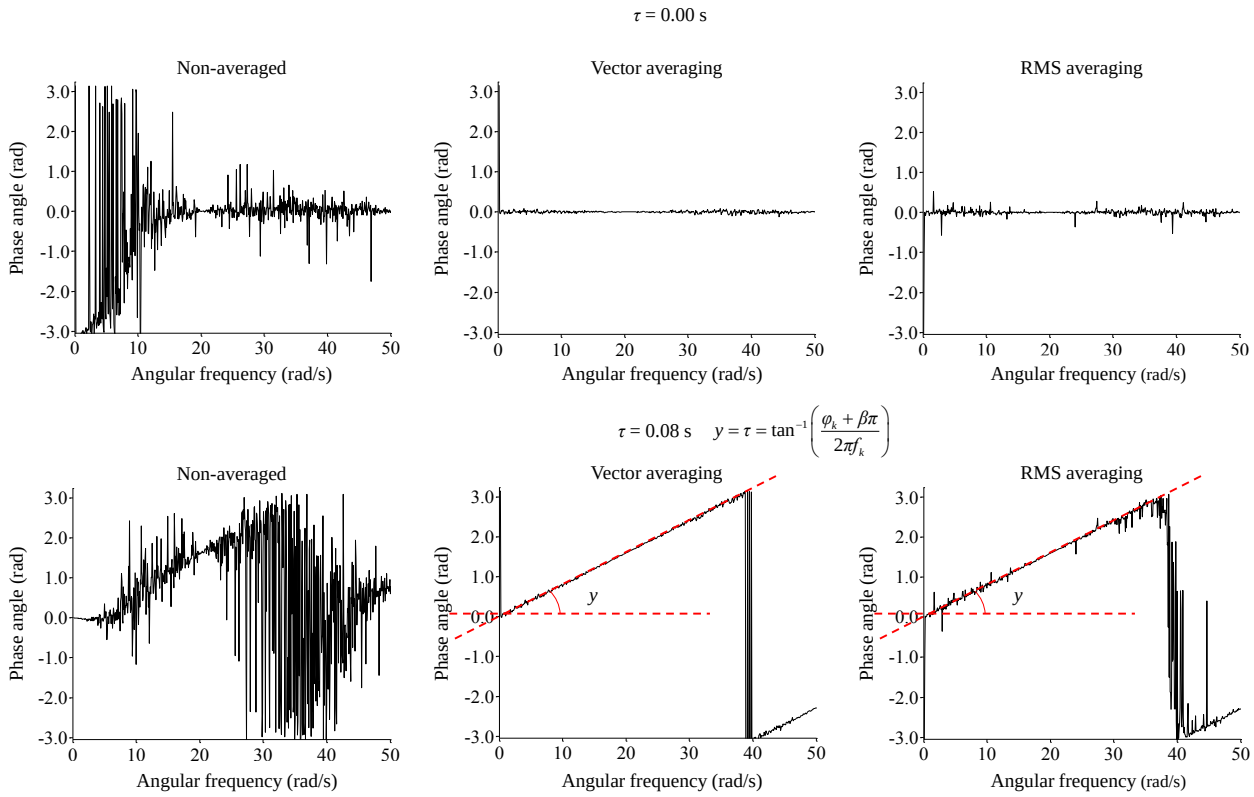

Figure 4: Effect of averaging on the spectral density phase angles.

3.3. Applicability limits of time lag detection

Due to the approximative nature of the FD-Sync approach, the limitations in terms of time lag detection are investigated through the simulations TS_1 and TS_2. The simulations address all possible sources of inaccuracies, including noise, FFT approximations, and non-proportional damping. Furthermore, since time lag detection relies on the cross spectral density phase angle φ_k, and, by extension, to the resolution of frequency bins, it is expected that the lowest detectable time lag cannot be lower than the time interval $\Delta t = 1/f_s$, where f_s is the sampling frequency. Finally, even after applying the noise reduction method described in Section 3.2, residual noise levels could still offset cross spectral density phase angles from their actual values. Since Equation 22 essentially relates time lag τ with the slope of the cross spectral density phase spectrum, relatively large offsets of φ_k might compromise the accuracy of time lag detection. To avoid offset-induced inaccuracies, instead of applying Equation 22 directly, the linear trend (slope) of the cross spectral density phase spectrum, shown in Figure 4, is estimated using linear regression, and the slope of the linear regression curve is considered to be equal to time lag τ.

Since the purpose of the FD-Sync approach is to enable obtaining correct modal information from structural response data, the effect of time lags on the mode shapes of the 5-DOF oscillator needs to be investigated. According to Krishnamurthy et al. [8], the extraction of experimental mode shapes could be affected by time lags as short as 10 μs; however, it is argued that the effect of

synchronization discrepancies should case-specifically be estimated according to the bandwidth of interest. In this study, to showcase this effect, preliminary simulations of the oscillator are conducted, by injecting random time lags of increasing length (ranging from 0.001 s to 0.1 s) into the signals representing the structural response data. As a metric to quantify the effect, mode shapes ψ_u are extracted from the unsynchronized signals and are compared to the original mode shapes ψ_o, using the modal assurance criterion (MAC) [44]:

$$\mathrm{MAC}\{\psi_u, \psi_o\} = \frac{\left|\psi_u^T \cdot \psi_o\right|^2}{\left(\psi_u^T \cdot \psi_u\right) \cdot \left(\psi_o^T \cdot \psi_o\right)}. \tag{29}$$

Similarity between ψ_u and ψ_o is indicated by MAC values close to 1, while loss of similarity occurs for values below 0.9 [45]. Figure 5 summarizes the MAC values for different ranges of time lags and for all 5 vibration modes of the oscillator.

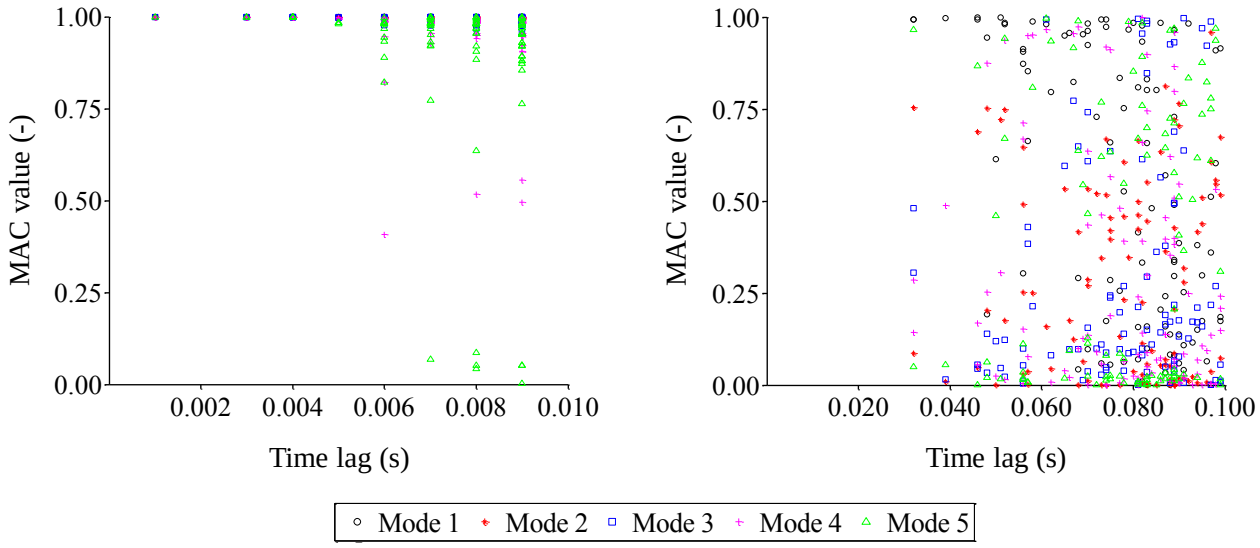

Figure 5: Effect of time lags of vibration modes of the 5-DOF oscillator.

As can be seen in Figure 5, the 4th and 5th vibration modes are more sensitive to short time lags, which is expected since high-order vibration modes have shorter periods. Nevertheless, time lags shorter than 5 ms seem to have a negligible effect on all vibration modes. By contrast, time lags longer than 10 ms result in MAC values lower than 0.9 in most cases. As a result, the lowest time lag to be considered for the simulations TS_1 and TS_2 is set to 1 ms, which is expected to adequately illustrate the efficacy of the FD-Sync approach.

In both sets of the simulations TS_1 and TS_2, upon computing the structural responses of the oscillator for each simulation, a series of time lags, ranging between -500 ms and 500 ms with a 1 ms step, are artificially inserted into the signals corresponding to the structural response data of degrees of freedom x_2, x_3, x_4, and x_5. Subsequently, the time lag detection is performed by estimating the linear trend of the cross spectral density phase spectra between pairs of signals x_1-

x_2, x_1-x_3, x_1-x_4, x_1-x_5. To investigate the effects of the time interval Δt and of noise reduction, 5 sampling frequencies are considered, and 3 analysis lengths. For each sampling frequency, a different window size is selected for windowing with an overlap of 50%. The simulation parameters for both sets of simulations are summarized in Table 2.

Table 2: Simulation parameters.

Sampling frequency f_s (Hz)	Analysis length (number of points)			Window size (number of points)
	10 min	1 h	24 h	
12.5	7,500	45,000	1,080,000	1,024
25	15,000	90,000	2,160,000	2,048
50	30,000	180,000	4,320,000	4,096
100	60,000	360,000	8,640,000	8,192
512	307,200	1,843,200	44,236,800	32,768

The results from the simulations TS_1 and TS_2 are summarized in the following figures. As a metric of efficacy, each time lag detected, τ_d, is plotted against the corresponding time lag inserted, τ_i. The proximity between τ_d and τ_i is demonstrated through the distance of τ_d from an idealized curve, corresponding to $\tau_d = \tau_i$, represented in the figures as a dashed line.

Figure 6 illustrates the effect of the sampling frequency on time lag detection both for proportional damping (TS_1) and non-proportional damping (TS_2) for an analysis length of 1 h. The results are shown for time lags inserted in the signal of DOF x_2 and for the FD-Sync being applied on the cross spectral density phase spectrum between signals from DOF x_1 and DOF x_2.

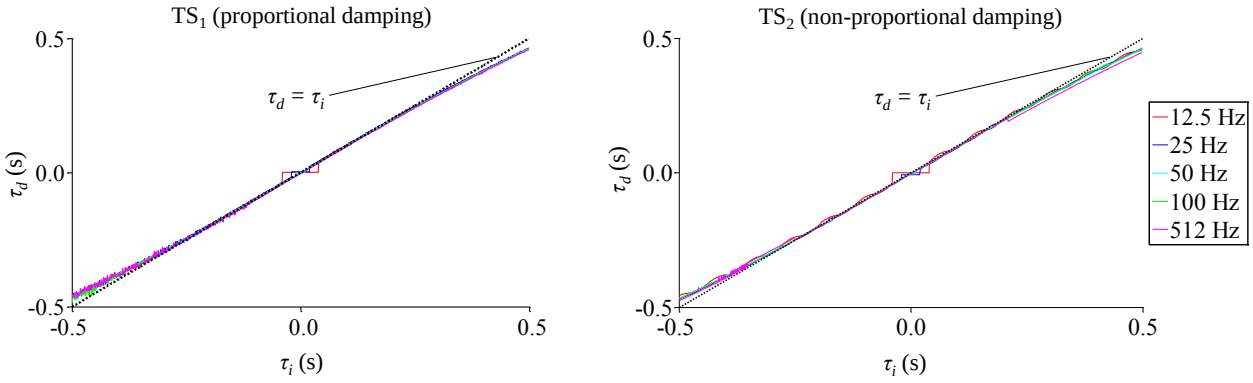

Figure 6: Effect of the sampling frequency on the time lag detection between DOF pairs x_1-x_2 for analysis length of 1 h :TS_1 – proportional damping (left) and TS_2 – non-proportional damping (right).

In Figure 7, the effect of the analysis length is shown for the same pairs of degrees of freedom as in Figure 6, and for f_s = 100 Hz, and Figure 8 depicts the performance of the FD-Sync approach when applied to all DOF pairs analyzed, i.e. x_1-x_2, x_1-x_3, x_1-x_4, x_1-x_5.

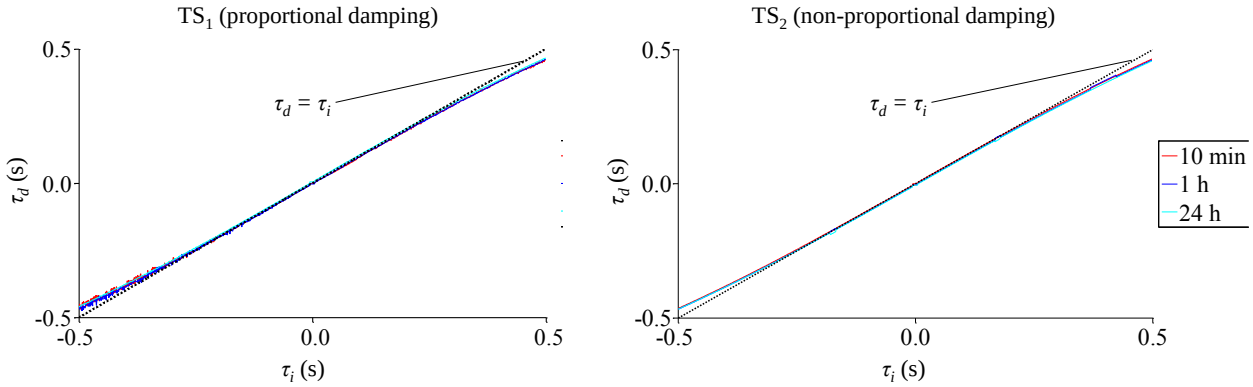

Figure 7: Effect of the analysis length on the time lag detection between DOF pairs x_1-x_2 for a sampling frequency of 100 Hz: TS_1 – proportional damping (left) and TS_2 – non-proportional damping (right).

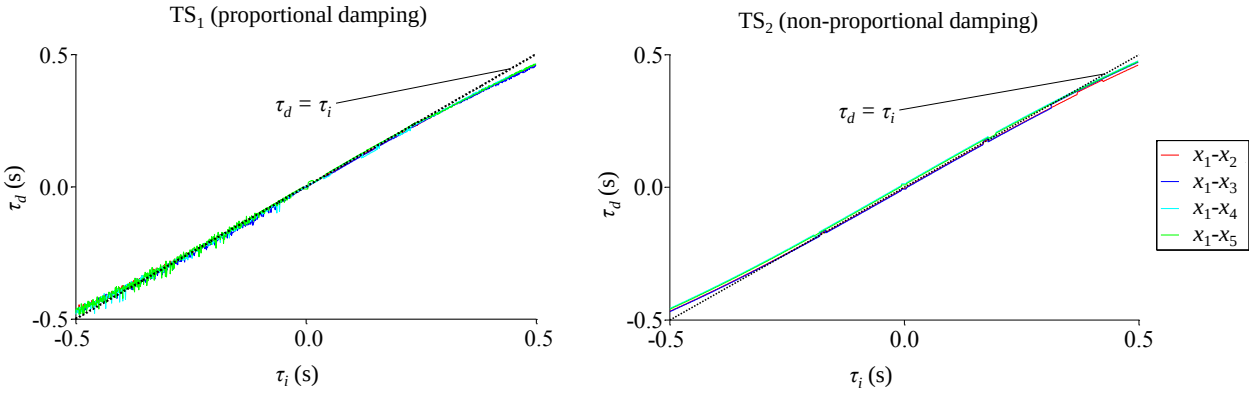

Figure 8: Time lag detection between all DOF pairs analyzed for a sampling frequency of 100 Hz and an analysis length of 1 h: TS_1 – proportional damping (left) and TS_2 – non-proportional damping (right).

The results of the simulations TS_1 and TS_2 showcase the capability of the FD-Sync approach to detect time lags within a range of ±300 ms with low errors, regardless of sampling frequency, analysis length, and the existence of random phase shifts. For time lags longer than 300 ms, the time lag detection quality deteriorates; however, the error remains relatively low in almost all cases. Therefore, in case time lags detected with the FD-Sync approach exceed 300 ms, it is recommended that the approach is repeated more than once to obtain optimal results. Furthermore, in Figure 6, large errors are observed for low sampling frequencies and time lags close to zero. These errors are attributed to time lags being shorter than the time step of the respective signals and are detected as zero time lags, i.e. the corresponding cross spectral density phase function is relatively "flat" similar to Figure 4 for τ = 0.00 s. Taking the aforementioned limitations into consideration, the validation tests of the FD-Sync approach are presented in the next section.

4. Validation tests on a road bridge

The proposed FD-Sync approach is validated using SHM data from field tests on a road bridge equipped with a SHM system. First, the road bridge and the SHM system are briefly described. Next, the validation tests are presented and the results are discussed.

4.1. Description of the road bridge and the SHM system

The road bridge selected for the validation tests is the Infante Dom Henrique Bridge spanning River Douro and connecting the cities of Porto and Gaia in Portugal, shown in Figure 9. The bridge has a total length of 371 m and consists of a prestressed concrete deck resting on a reinforced concrete arch of length 280 m and height 25 m. The deck features a box girder cross section with a depth of 4.50 m, and the arch has a rectangular cross section with constant 1.50 m thickness and width that varies linearly from 20 m at the arch ends to 10 m at the midspan. At the central part of the bridge, the deck is adjoined to the arch for a length of 70 m about the midspan, essentially forming a 6.00 m deep box girder. Across the rest of the bridge length, the arch is connected to the deck via equidistant piers at 35 m up to the abutments. The headroom of the bridge is 75 m.

Figure 9: Infante Dom Henrique Bridge in Portugal.

The SHM system installed on the bridge comprises 4 groups of accelerometers attached at 4 locations across the bridge deck [46], as shown in Figure 10. Each group of accelerometers consists of 2 accelerometers measuring at the vertical (z) direction, symmetrically positioned with respect to the longitudinal axis of the deck, and one accelerometer measuring at the transversal (y) direction. The acceleration response data is collected over a period of one year at a sampling

frequency of 50 Hz. As discussed in [46], the most significant vibration modes of the bridge lie within the range of 0-5 Hz; therefore, the acceleration response data is downsampled to 12.5 Hz.

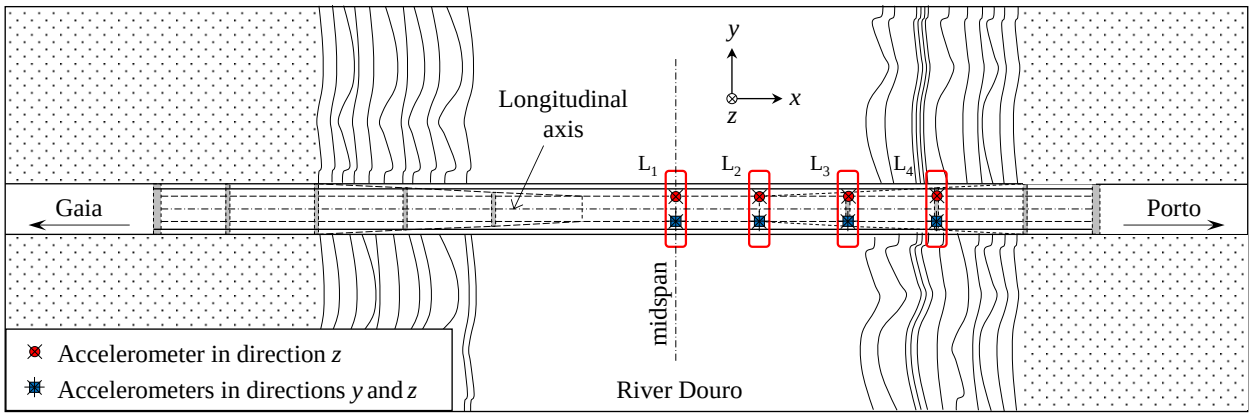

Figure 10: SHM system installed at the Infante Dom Henrique Bridge.

The validation tests are designed with a similar concept as simulations TS_1 and TS_2. Since the FD-Sync approach relies on the cross spectral density phase, it follows that the SHM data records, containing acceleration response data, need to exhibit similar frequency content, which may not always apply if the records are from different measuring directions. Hence, in this study, only the 8 SHM data records in the z direction are considered, corresponding to the positions $L_{i,o}$ and $L_{i,u}$ ($i = 1…4$) with "o" and "u" depicting the locations over and under the longitudinal axis of the deck. The length of the SHM data records used in the validation tests is one day (24 h). In each analysis, the SHM data record $x_{1,u}$ from location $L_{1,u}$ serves as reference and is kept in its original form. Artificial time lags (τ_i), ranging from -560 ms to 560 ms, are sequentially inserted into the rest of the SHM data records $x_{j,u}$ from locations $L_{j,u}$ ($j = 2…4$) and $x_{i,o}$ from locations $L_{i,o}$ ($i = 1…4$) and detected (τ_d) through the slope of the cross spectral density phase spectrum with record $x_{1,u}$. The step for inserting the time lags is set to 80 ms, coinciding with the sampling frequency of the SHM data. Vector averaging is applied in each analysis with a window size of 1,024 measurements and an overlap of 50 %. The results are illustrated in Figure 11, and the root mean square errors (RMSE) between τ_d and τ_i for all locations are summarized in Table 3. The time lag estimation through the slope of the cross spectral density phase spectrum is exemplarily shown in Figure 12 for two time lag values.

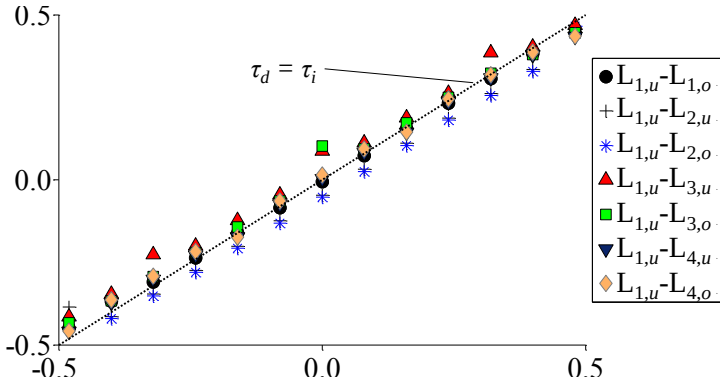

Figure 11: Time lag detection between all measurement locations of the SHM system installed on Infante Dom Henrique Bridge for a sampling frequency of 12.5 Hz and an analysis length of 24 h.

Table 3: Root mean square errors between inserted time lags and detected time lags.

Location	RMSE (s)
$L_{1,u}$-$L_{1,o}$	0.026
$L_{1,u}$-$L_{2,u}$	0.053
$L_{1,u}$-$L_{2,o}$	0.054
$L_{1,u}$-$L_{3,u}$	0.053
$L_{1,u}$-$L_{3,o}$	0.040
$L_{1,u}$-$L_{4,u}$	0.027
$L_{1,u}$-$L_{4,o}$	0.029

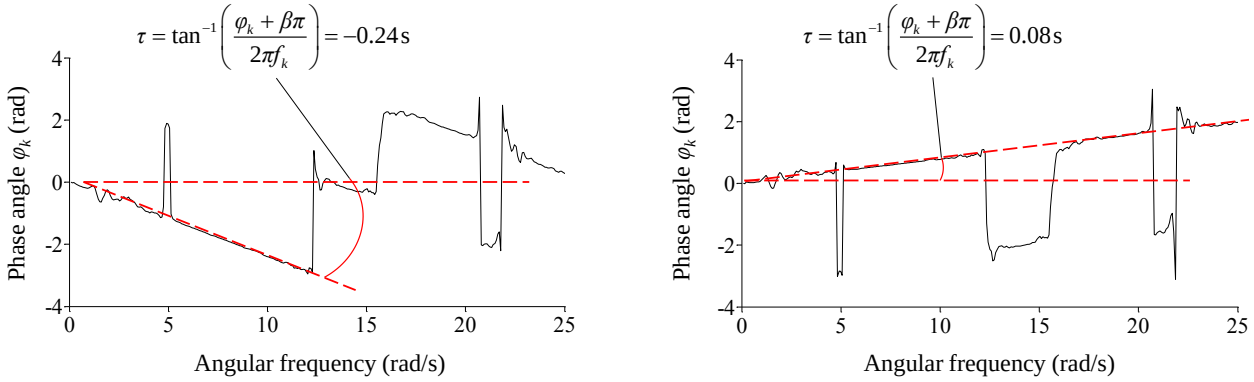

Figure 12: Exemplary time lag estimation through the slope of the cross spectral density phase function for τ = -0.24 s (left) and τ = 0.08 s (right).

The results of the validation tests corroborate the observations from simulations TS_1 and TS_2 for real-world SHM data. Specifically, the FD-Sync approach exhibits high efficacy for time lags up to 300 ms, which represent realistic synchronization discrepancies in modern SHM systems, with errors generally lower than 10 ms. For time lags longer than 300 ms, the quality of the FD-Sync approach deteriorates with errors exceeding 50 ms. Therefore, to increase the accuracy of time lag detection, it is recommended to repeat the FD-Sync approach more than once, in case time lags longer than 300 ms are detected. Furthermore, as shown in Figure 11, offsets between time lags may be observed regardless of the length of the time lags, e.g. between locations $L_{1,u}$ and $L_{2,u}$. These offsets may be attributed to slight differences in the frequency contents of the respective data

records due, for example, to frequency components having low amplitudes in some locations. It is therefore recommended to apply the FD-Sync approach multiple times with different reference data records to enhance the robustness of time lag detection. Finally, the validation tests demonstrate that the proposed approach is independent from the type of vibration mode. In other words, although the setup of sensors in the SHM system results in frequency contents including translational as well as torsional vibration modes, the capability of the FD-Sync approach to estimate time lags remains unaffected.

5. Summary and conclusions

In structural health monitoring, vibration-based outcomes may be compromised by synchronization discrepancies. Specifically, loss of synchronization affects the phase differences between SHM data records, which, in turn, results in poorly estimated mode shapes. Synchronization discrepancies predominantly affect wireless SHM systems, in which wireless sensor nodes with no centralized clock management are used. In addition, cable-based SHM systems may also exhibit synchronization discrepancies in case multiple data acquisition units are used. This paper has presented a frequency-domain synchronization approach for vibration-based SHM. The proposed approach builds upon the relationship of cross spectral density phases between two SHM data records of acceleration response data with time lags between the records. As has been proven in this paper, the slope of the cross spectral density phase spectrum may mathematically be related to the time lags between the records.

The frequency-domain synchronization approach has been verified through simulations of a 5-DOF oscillator under white noise excitation, in which the capabilities and limitations of the approach have been investigated. Specifically, it has been observed that it is capable of yielding reliable estimates of time lags up to 300 ms with low errors, regardless of sampling frequency, analysis length, and measurement location. Moreover, it has been demonstrated that time lag estimation with the proposed approach is not affected by phase shifts between SHM data records, occurring as a result of non-proportional damping. Finally, the efficacy of the frequency-domain synchronization approach has been validated through tests using data from a real-world SHM system installed on a road bridge in Portugal. The results from the validation tests have corroborated the observations from the simulations with respect to the limitations of time lag estimation and to the capability of the frequency-domain synchronization approach to estimate time lags up to 300 ms with low errors. Future work will focus on automating and embedding frequency-domain synchronization approach in wireless sensor nodes. Furthermore, the favorable effect of the approach on correcting mode shapes will be examined in structures with responses in variable frequency bandwidths.

6. Acknowledgments

The authors of this collaborative research endeavor gratefully acknowledge the support offered by the German Research Foundation (DFG) through grants SM 281/14-1 and SM 281/20-1. This work was also financially supported by Programmatic funding UIDP/04708/2020 of the CONSTRUCT – "*Instituto de I&D em Estruturas e Construções*" and the project PTDC/ECI-EST/29558/2017, both funded by the Portuguese Foundation of Science and Technology/Ministry of Science, Technology and Higher Education (FCT/MCTES) under the Central Administration Program for Investments and Expenses on Development (PIDDAC). Any opinions, findings, conclusions, or recommendations expressed in this paper are those of the authors and do not necessarily reflect the views of the DFG or the FCT/MCTES.

7. References

[1] Anderegg, P., Brönimann, R. and Meier, U. (2014). "Reliability of long-term monitoring data". *Journal of Civil and Structural Health Monitoring*, 4(1): 69-75.

[2] Kullaa, J. (2010). "Vibration-based structural health monitoring under variable environmental or operational conditions". In: Deraemaeker, A. and Worden K. (eds), *New Trends in Vibration Based Structural Health Monitoring*, Udine, Italy : SpringerWienNewYork. Pp. 107-182.

[3] Smarsly, K. and Law, K.H. (2014). "Decentralized fault detection and isolation in wireless structural health monitoring". *Advances in Engineering Software*, 73(2014): 1-10.

[4] Lynch, J.P. and Loh, K.J. (2006). "A summary review of wireless sensors and sensor networks for structural health monitoring". *The Shock and Vibration Digest*, 38(2): 91-128.

[5] Nguyen, T., Chan, T.H.T., Thambiratnam, D.P. and King, L. (2015). "Developments of a cost-effective flexible vibrations DAQ system for long-term continuous structural health monitoring". *Mechanical Systems and Signal Processing*, 64-65(2015): 313-324.

[6] Tavares Bruscato, L., Heimfarth, T. and De Freitas, E.P. (2017). "Enhancing time synchronization support in wireless sensor networks". *Sensors*, 17(12): 2956.

[7] Scuro, C., Sciammarella, P.F., Lamonaca, F., Olivito, R.S. and Carnì, D.L. (2018). "IoT for Structural Health Monitoring". *IEEE Instrumentation & Measurement Magazine*, 21(6): 4-14.

[8] Krishnamurthy, V., Fowler, K. and Sazonov, E. (2008). "The effect of time synchronization of wireless sensors on the modal analysis of structures". *Smart Materials and Structures*, 17(2018): 055018.

[9] Li, Q. and Rus, D. (2006). "Global clock synchronization in sensor networks". *IEEE Transactions on Computers*, 55(2): 214-226.

[10] Swain, A.R. and Hansdah, R.C. (2015). "A model for the classification and survey of clock synchronization protocols in WSNs". *Ad Hoc Networks*, 27(2015): 219-241.

[11] Elson, J., Girod, L. and Estrin, D. (2002). "Fine-grained network time synchronization using reference broadcasts". *ACM SIGOPS Operating Systems Review*, 36(SI): 147-163.

[12] Ganeriwal, S., Kumar, R. and Srivastava, M.B. (2003). "Timing-sync protocol for sensor networks". In: *Proceedings of the 1st International Conference on Embedded Networked Sensor Systems*, Los Angeles, CA, USA, 05/11/2003.

[13] Maróti, M., Kusy, B., Simon, G. and Lédeczi, Á. (2004). "The flooding time synchronization protocol". In: *Proceedings of the 2nd International Conference on Embedded Networked Sensor Systems*, Baltimore, MD, USA, 03/11/2004.

[14] Chauhan, S. and Awasthi, L.K. (2012). "Adaptive time synchronization for homogeneous WSNs". *International Journal of Engineering Business Management*, 4(2012): 54898.

[15] Sommer, P. and Wattenhofer, R. (2009). "Gradient clock synchronization in wireless sensor networks". In: *Proceedings of the International Conference on Information Processing in Sensor Networks*, San Fransisco, CA, USA, 13/04/2009.

[16] Yildirim, K.S. and Gürcan, Ö. (2014). "Efficient time synchronization in a wireless sensor network by adaptive value tracking". *IEEE Transactions on Wireless Communications*, 13(7): 3650-3664.

[17] Li, J., Mechitov, K., Kim, R.E. and Spencer Jr, B.F. (2016). "Efficient time synchronization for structural health monitoring using wireless smart sensor networks". *Structural Control Health Monitoring*, 23(3): 470-486.

[18] Rice, J. and Spencer Jr, B.F. (2009). "Flexible smart sensor framework for autonomous full-scale structural health monitoring". *NSEL Report No. 018*, University of Illinois at Urbana-Champaign.

[19] Nagayama, T., Spencer Jr, B.F. and Rice, J.A. (2009). "Autonomous decentralized structural health monitoring using smart sensors". *Structural Control Health Monitoring*, 16(7-8): 842-859.

[20] Wang, Y., Lynch, J.P. and Law, K.H. (2007). "A wireless structural health monitoring system with multithreaded sensing devices: design and validation". *Structure and Infrastructure Engineering*, 3(2): 103-120.

[21] Bocca, M., Eriksson, L.M., Mahmood, A., Jäntti, R. and Kullaa, J. (2011). "A synchronized wireless sensor network for experimental modal analysis in structural health monitoring". *Computer-Aided Civil and Infrastructure Engineering*, 26(7): 483-499.

[22] Lei, Y., Kiremidjian, A.S., Nair, K.K., Lynch, J.P. and Law, K.H. (2005). "Algorithms for time synchronization of wireless structural monitoring sensors". *Earthquake Engineering and Structural Dynamics*, 34(6): 556-573.

[23] Sazonov, E., Krishnamurthy, V. and Schilling, R. (2010). "Wireless intelligent sensor and actuator network – A scalable platform for time-synchronous applications of structural health monitoring". *Journal of Structural Health Monitoring*, 9(5): 465-476.

[24] Chintalapudi, K., Fu, T., Paek, J., Kothari, N., Rangwala, S., Caffrey, J., Govindan, R., Johnson, E. and Masri, S. (2006). "Monitoring civil structures with a wireless sensor network". *IEEE Internet Computing*, 10(2): 26-34.

[25] Severino, R., Gomes, R., Alves, M., Sousa, P., Tovar, E., Ramos, L.F., Aguilar, R. and Lourenco, P.B. (2010). "A wireless sensor network platform for structural health monitoring: enabling accurate and synchronized measurements through COTS + custom-based design". In: *Proceedings of the 5th IFAC Conference on Management and Control of Production Logistics*, Coimbra, Portugal, 08/09/2010.

[26] Federici, F., Alesii, R., Coliareti, A., Faccio, M., Graziosi, F., Gattulli, V. and Potenza, F. (2014). "Design of wireless sensor nodes for structural health monitoring applications". *Procedia Engineering*, 87(2014):1298-1301.

[27] Hu, X. and Wang, B. (2013). "A wireless sensor network-based structural health monitoring system for highway bridges". *Computer-Aided Civil and Infrastructure Engineering*, 28(3): 193-209.

[28] Tan, C., Ji, S., Gui, Z., Shen, J., Fu, D.-S. and Wang, J. (2018). "An effective data fusion-based routing algorithm with time synchronization support for vehicular wireless sensor networks". *The Journal of Supercomputing*, 74(2018): 1267-1282.

[29] Fu, H., Khodaei, Z.S. and Aliabadi, M.H.F. (2020). "Synchronized wireless sensors for aircraft structural health monitoring". In: *Proceedings of the 19th International Conference on Fracture and Damage Mechanics*, 15/09/2020.

[30] Val, I., Arriola, A., Cruces, C., Torrego, R., Gomez, E. and Arizkorreta, X. (2015). "Time-synchronized wireless sensor network for structural health monitoring applications in railway environments". In: *Proceedings of the IEEE World Conference on Factory Communication Systems*, Palma de Mallorca, Spain, 16/07/2015.

[31] Nagayama, T., Sim, S.H., Miyamori, Y. and Spence Jr., B.F. (2007). "Issues in structural health monitoring employing smart sensors". *Smart Structures and Systems*, 3(3): 299-320.

[32] Li, Q. and Rus, D. (2006). "Global clock synchronization in sensor networks". *IEEE Transactions on Computers*, 55(2): 214-226.

[33] Brincker, R. and Brandt, A. (2011). "Time synchronization by modal correlation". In: Proceedings of the 4th *International Operational Modal Analysis Conference*, Istanbul, Turkey, 09/05/2011.

[34] Maes, K., Reynders, E., Rezayat, A., De Roeck, G. and Lombaert, G. (2016). "Offline synchronization of data acquisition systems using system identification". *Journal of Sound and Vibration*, 381(2016): 264-272.

[35] Dragos, K., Theiler, M., Magalhães, F., Moutinho, C. and Smarsly, K. (2018). "On-board data synchronization in wireless structural health monitoring systems based on phase locking". *Structural Control and Health Monitoring*, 25(11), e2248.
[36] Dragos, K., Makarios, T., Karetsou, I., Manolis, G. D., and Smarsly, K. (2020). "Detection and correction of synchronization-induced errors in operational modal analysis". *Archive of Applied Mechanics*, 90(7): 1547-1567.
[37] Bernal, D. (2018). "Analytical minimization of synchronicity errors in stochastic identification". *Mechanical Systems and Signal Processing*, 98(1): 415-424.
[38] Diord, S., Magalhães, F., Cunha, Á. and Caetano, E. (2017). "High spatial resolution modal identification of a stadium suspension roof: Assessment of the estimates uncertainty and of modal contributions". *Engineering Structures*, 135(2017): 117-135.
[39] Dragos, K. and Smarsly, K. (2016). "Distributed adaptive diagnosis of sensor faults using structural response data". *Smart Materials and Structures*, 25(10): 105019.
[40] Magalhães, F., Cunha, Á., Caetano, E. and Brincker R. (2010). "Damping estimation using free decays and ambient vibration tests". *Mechanical Systems and Signal Processing*, 24(5): 1274-1290.
[41] Den Hartog, J. P. (1985). "Mechanical vibrations". Mineola, NY, USA: Dover Publications.
[42] Brincker, R. and Zhang, L. (2009). "Frequency domain decomposition revisited". In: *Proceedings of the 3rd International Operational Modal Analysis Conference*, Portonovo, Italy, 04/05/2009.
[43] Witte, R.A. (2006). "Spectrum and network measurements". Raleigh, NC, USA: Scitech Publishing, Inc.
[44] Allemang, R.J. (2003). "The modal assurance criterion - Twenty years of use and abuse". *Journal of Sound and Vibration*, 37(8): 14-23.
[45] Pastor, M., Binda, M. and Harčarik, T. (2012). "Modal assurance criterion". *Procedia Engineering*, 48(2012):543-548.
[46] Magalhães, F., Cunha, Á. And Caetano, E. (2012). "Vibration based structural health monitoring of an arch bridge: From automated OMA to damage detection". *Mechanical Systems and Signal Processing*, 28(2012): 212-228.